The Development of an Overset/Hybrid Method For Rotorcraft Applications

Ashok K. Bangalore and Marvin A. Moulton
Research Scientist
Flow Analysis, Inc.
NASA Ames Research Center

Francis X. Caradonna
Staff Scientist
Army/NASA Rotorcraft Division
US Army AvRDEC (AMCOM)
NASA Ames Research Center

Abstract

This paper describes the development of an overset/hybrid computation scheme for the prediction of general rotor/wake flows. The method combines a viscous flow solver near the blade surface with a vorticity embedding, potential method in the far-field. The blade flow region is computed using a local hybrid method consisting of combined viscous and potential solvers that employ a body-fitted, C-topology. The outer wake region is solved by a vorticity embedding, potential method that uses an H-topology. The blade and wake regions are coupled by oversetting. The overall approach is intended for application to all flight modes. Critical elements of the method are applied to unsteady flows and forward flight for the first time in this paper. Computations shown include the applications of hybrid and hybrid/overset methods to hover. Next, an unsteady isolated blade hybrid method, utilizing an external wake inflow model, is applied to advancing rotors. Then, an unsteady overset method is employed to solve the near blade aerodynamics as well as the far-field wake of a four-bladed rotor in forward flight. Finally, the overset method is applied to the classical pitching and plunging airfoil problems in order to assess moment prediction capability.

Nomenclature

C_T = gross thrust coefficient
C_t = sectional thrust coefficient, $C_\ell c(r)(r/R)^2$
C_n = sectional normal force coefficient
C_l = sectional lift coefficient
C_m = sectional pitching moment coefficient
$c(r)$ = chord length
c_r = reference chord length
h = cell volume
M_T = hover tip Mach number
n = time level
$\vec{q}$ = total velocity
$\vec{q}^v$ = vortical velocity
R = rotor tip radius
Re_c = Reynolds number based on root chord
r = radial location
U, V, W = contravariant velocity components in the $\xi-$,$\eta-$ and $\zeta-$ directions, respectively
u, v, w = velocity components in the $x-$,$y-$ and $z-$ directions, respectively
x, y, z = Cartesian coordinates
Γ = bound circulation
λ = shape function used in wake modeling
ξ, η, ζ = generalized computational coordinates
ρ = density
μ = advance ratio
τ = time in computational domain
θ_c = collective pitch
ϕ = velocity potential
Ψ = azimuth angle

Subscripts

t = real time
x, y, z = pertaining to Cartesian coordinates
i, j, k = pertaining to grid indices

Presented at the American Helicopter Society Technical Specialists' Meeting For Rotorcraft Aerodynamics and Aeroacoustics, Williamsburg, Virginia, October 27 - 30, 1997.

Introduction

For many years, the Computational Fluid Dynamics (CFD) community has been developing methods aimed at ultimately predicting the entire flow about helicopter rotors, including transonic, viscous and wake effects. The first use of CFD in full rotor computations involved coupling the then newly developed unsteady transonic codes [1-5] with a vortex-lattice representation of the wake to compute the near-blade aerodynamics. Further on, work was attempted to unify the prediction of the rotor-wake aerodynamics by solving approximations to the Navier-Stokes equations for the entire flowfield and capturing the wake from first principles. For example, Bangalore [6] and Ahmad et al. [7] have used viscous solvers to obtain forward flight solutions. These methods capture the rotor wake as part of the solution process. However, the numerical dissipation inherent in the Navier-Stokes methods result in excessive diffusion of the wake. Hence, viscous solvers require very fine grids to resolve the wake and are therefore impractical given current computational resources.

Vorticity embedding is the first successful CFD method for the non-dissipative treatment of the shed rotor wake. This method is unique among CFD methods because it preserves the identity of wake circulation without requiring dense grids. The circulation is not carried by the grid but rather by a sheet of convecting markers whose circulation is then impressed on the adjacent grid points as a local vortical velocity distribution. This method has been successfully implemented in the HELIX-I code [8] to predict hover performance as well as in the HELIX-II code [9] to demonstrate its applicability to model the rotor wake in forward flight cases. Since vorticity embedding is a potential-based method, viscous regions of the flowfield cannot be addressed.

Both the Navier-Stokes and vorticity embedding methods described above individually solve a single set of flow equations in an attempt to compute the entire rotor flowfield. Our approach is to develop hybrid methods that combine a near blade viscous solver with a vorticity embedding, potential solver away from the blade to convect the rotor wake. For hover, Moulton et al. [10] developed a hybrid method which utilizes coincident C-topologies. Significant errors in the convection of the wake markers were found and attributed to the far field C-topology. Therefore, a potential-based overset method was developed that combines a C-topology with a background H-topology [11]. The C-topology was subsequently hybridized with an inner viscous solver which results in an overset/hybrid method.

Development of the overset/hybrid method for hover was facilitated by individually examining some essential elements of the overall procedure. This same strategy is used to assemble an unsteady overset/hybrid method. This paper describes the current state of development of these elements for the prediction of advancing rotor flows. In particular, an unsteady hybrid code is developed that couples an inner viscous solver with an outer vorticity embedding, potential solver. In addition, a potential-based, unsteady overset method is developed and combines a near surface C-topology with a background H-topology.

Physical Models

This section gives a brief explanation of the flow solvers used in the viscous and inviscid zones of the hybrid scheme. The vorticity embedding concept is explained in the inviscid zone description. The salient features of the numerical algorithms used in each zone are discussed.

Viscous Zone

The viscous zone was modeled using TURNS (Transonic Unsteady Rotor Navier-Stokes) [12]. In this code, the inviscid fluxes are computed using an upwind-biased flux-difference scheme with flux limiters to model shocks. There is no need for explicit numerical dissipation with the use of upwinding. The flux limiters lead to a TVD (total variation diminishing) scheme which improves the spatial accuracy to second- or third-order. The implicit operator is solved using a Lower-Upper-Symmetric Gauss-Seidel scheme.

Inviscid Zone

The inviscid flow is governed by the unsteady, potential equation, written in generalized coordinates,

$$\begin{array}{rcl} \frac{\partial \rho}{\partial \tau} & + & \frac{\partial}{\partial \xi}(\rho h U) \\ & + & \frac{\partial}{\partial \eta}(\rho h V) + \frac{\partial}{\partial \zeta}(\rho h W) = 0 \end{array} \qquad (1)$$

where the contravariant velocities (U, V, W) are defined as

$$\begin{array}{l} U = \xi_t + \xi_x u + \xi_y v + \xi_z w \\ V = \eta_t + \eta_x u + \eta_y v + \eta_z w \\ W = \zeta_t + \zeta_x u + \zeta_y v + \zeta_z w. \end{array} \qquad (2)$$

Note that ξ_t , ξ_x , ξ_y , ξ_z , etc. are the primitive metrics of the transformation, and h is the cell volume. The physical velocity components are given by

$$\vec{q} = \nabla \phi + \vec{q}^{\,v} \qquad (3)$$

where $\vec{q}^{\,v}$ corresponds to the vortical velocity which is a result of the vorticity embedding technique and is explained below.

The unsteady potential equation, along with vorticity embedding, is solved using a semi-implicit, finite-volume scheme. The computer code is called HELIX-II [9] which utilizes H-topologies to predict advancing rotor flows. The most attractive feature of HELIX-II is the inclusion of vorticity embedding to freely convect the shed rotor wake.

The basis of the vorticity embedding method is to decompose the velocity into potential and rotational components,

$$\vec{q} = \nabla\phi + \vec{q}^{\,v} = \nabla\phi + \Gamma\nabla\lambda \qquad (4)$$

where Γ (circulation) and λ are Clebsch variables and represent the local strength and geometry of the shed wake, respectively. This decomposition introduces a forcing term into the standard potential equation.

The idea is to spread an infinitesimally thin vortex sheet (the usual potential model) into a finite thickness vorticity layer. The internal structure of this layer is unimportant since it is thin compared with other length scales of the problem. The first step in this process is to determine the wake geometry. Along the rotor span, the wake is represented by a set of nodes uniformly distributed around the azimuth. The azimuthal node intervals are determined from the time step used for the calculation. Radial nodes are located at grid cell centers. The wake convection procedure involves the following steps:

1. inertial coordinates of the blade fixed grid corresponding to the new time step are obtained
2. a new set of marker nodes is added at the updated blade trailing edge location
3. all wake nodes are displaced to follow the local flow

In general, the wake node locations do not coincide with the Eulerian grid points. Therefore, the local velocity at the node is determined by trilinear interpolation of the velocities at the surrounding grid points.

Once the wake geometry is obtained for a given time step, the circulation of the convecting Lagrangian wake nodes are impressed on the adjacent grid points as a local vortical velocity distribution. Since this procedure is completely described in Ref. 9, only a brief description is given here. The idea is to determine the Eulerian grid points that fall within a specified sphere of influence of each wake node. These points will receive a contribution from that segment of the wake sheet. This procedure is repeated for all wake nodes resulting in a shape parameter $\lambda_{i,j,k}$ and a strength parameter $\Gamma_{i,j,k}$ at these grid points. Upon defining the shape and strength of the vorticity field, the vortical velocity field is computed using

$$\vec{q}^{\,v} = \Gamma_{i,j,k}\nabla\lambda_{i,j,k} \qquad (5)$$

where $\vec{q}^{\,v}$ is the vortical velocity field and represents the vorticity in the shed wake. Since the wake is time dependent in forward flight, this process of computing the vortical velocity is required for each time step.

Boundary Conditions

Before describing the boundary conditions, clarification of terminology is in order. The term *hybrid* refers to the coupling of different equation sets, in this case potential with Navier-Stokes. When utilizing multiple grid topologies for the same equation set, the term *overset* will be used. For this research, a potential-based overset method is utilized to combine an inner C- with an outer H-grid. Further, hybridization of an overset code is called an overset/hybrid method.

Hybrid

The hybrid grid topology consists of a single block C-H grid topology that is constructed by stacking two-dimensional C-type grids in the radial direction. Off the tip of the blade, the grid is collapsed to form a double-line resulting in a beveled tip. The C-H grid topology is then decomposed into viscous and inviscid regions by specifying the outer location of the viscous zone and the number of overlap cells.

At the interface boundary of the viscous zone, a Dirichlet condition is provided by the full–potential solution. That is, the vector of conserved variables is constructed using the velocity field from the inviscid zone. The velocity potential on the interface boundary of the inviscid flow region is determined by integrating the velocity obtained from the viscous solution, a procedure similar to that of Berezin et al. [5].

Overset

The overset method utilizes two grid topologies. The first is an outer H-H grid topology which is used to accurately convect the shed wake. The second is a C-H grid topology which allows subsequent hybridization of an inner viscous solver to the potential solver along coincident grid lines. For this two-grid system, the H-topology contains grid points that fall within the outer boundary of the inner C-grid. These hole points are effectively skipped by using an IBLANKing technique [13]. Additional details regarding the hole punching procedure and the grid connectivity data structure information are given in Ref. 13. The velocity potential on the boundaries are updated by searching and interpolating (tri-linear) the solution from the complementary grid.

In addition to velocity potential information, the

complementary grids require the total velocity as well as the vortical velocity fields. The marker convection is performed on the outer H-grid. Therefore, the velocity field from the inner C-grid is interpolated to the background grid. Once the marker locations are determined, the vortical velocity field is constructed on the H-grid and subsequently interpolated to the inner grid.

Results

The results are separated into three sections. By examining previous hover results [10,11], the first section demonstrates the capabilities of both the hybrid and overset/hybrid techniques. The next section addresses critical steps in the assembly of an unsteady overset/hybrid method. The hybrid and overset methods are separately applied to advancing rotors. This represents the first application of these methods to unsteady flow. In the final section, an airfoil study is conducted to better understand the issues concerning pitching moment accuracy.

Hover

To demonstrate the capabilities of both the hybrid and overset/hybrid techniques, hover results are presented. Using the previously developed hybrid code [10], hover results for the AH-64A rotor blade are presented to emphasize the importance of utilizing an inner viscous code. Next, results for a hovering UH-60A rotor are analyzed to demonstrate the capability of the overset/hybrid method [11].

Hybrid: The hover performance ($M_T = 0.628$, $Re_c = 2.75 \times 10^6$) of the four-bladed Apache rotor was analyzed. A typical grid used in the zonal procedure has 213 points in the wrap-around direction (144 points on the surface), 46 points in the normal direction and 35 radial planes (25 on the blade). The far field boundaries are located at $0.75R$ above and below the rotor and $1.6R$ outboard. The outer boundary of the viscous zone was chosen to be $0.5c_r$ measured along a $\xi = \text{const}$ grid line radiating from the trailing edge at the tip of the blade. The overlap region, common to both zones, extends 2 grid cells into the viscous zone. The leading and trailing edge spacings are $0.002c(r)$ and $0.005c(r)$, respectively. The viscous grid is constructed with a minimum spacing of $0.00002c(r)$ in the normal direction. The radial spacing at the tip is $0.005R$.

The hybrid analysis was run at several collective pitch settings ($\theta_c = 9.0°$ to $13.0°$) to generate performance data. For all computations, the collective pitch was set to match experiment and rigid blades were assumed. Comparisons of the predicted performance with unpublished experimental data as well as HELIX-I results is shown in Fig. 1. The experimental results are shown as a band of data to reflect the scatter in the measurements. It is noteworthy that within the experimental thrust limit, the computations fall within the bounds of the data. However, as the thrust is increased beyond that of the experiment, the predicted performance of the rotor with the hybrid method begins to degrade. Examination of the flowfield in the vicinity of the tip reveals that at the higher thrust levels the flow is separated. The two-dimensional, non-interacting integral boundary layer solver, used in the standard version of HELIX-I is not valid for separated flow. Thus, an inner viscous solver is necessary to accurately predict the performance at very high thrust levels.

Overset/hybrid: To facilitate the development of the overall structure of the overset/hybrid method for hover, only inviscid flows have been examined. The flow about a four-bladed Sikorsky UH-60A rotor in hover($M_T = 0.628, \theta_c = 10.0°$) was computed using the overset/hybrid method.

Figure 2 shows the overset grid topologies near the rotor blade. The dotted lines represent the outer H-topology. The C-grid used in the potential calculation has 193 points in the wrap-around direction (145 points on the surface), 34 points in the normal direction and 32 radial planes (21 on the blade). Note that only the outer boundary points are shown in Fig. 2. The outer boundary is located approximately $1.5c_r$, in all directions, from the rotor blade. The inner Euler grid is a subset of the potential C-grid. That is, the outer boundary of the viscous zone was chosen to be $0.5c_r$ measured along grid lines radiating from the trailing edge. The overlap region, common to both zones, extends 2 grid cells into the viscous zone. The leading and trailing edge spacings are $0.002c(r)$ and $0.005c(r)$, respectively. Constant normal spacing, $0.002c(r)$, is employed on the surface. The radial spacing at the tip is $0.01R$.

Our experience has shown that the accuracy of the shed wake (strength and location) can be determined by examining the radial distribution of thrust on the rotor blade. This includes local effects, such as the tip vortex shed by the previous blade, as well as global effects which are related to the entire wake structure. The radial load distribution for this computation, Fig. 3, compares well with the experimental data of Lorber et al. [14]. Good prediction of tip loading indicates that the first passage of the tip vortex is well represented. Accuracy of the overall wake structure, tip vortices as well as inboard sheets, is demonstrated by good inboard load prediction. It is noteworthy that the quality of this comparison is typical for other collective pitch settings as well.

These results indicate that accurate representation

of the wake can be achieved using an overset/hybrid method. Qualitatively, the ability to predict near blade viscous effects was demonstrated using the hybrid method. Using our experience with developing an overset/hybrid method for hover, we have proceeded to construct the essential elements (hybrid and overset methods) for an unsteady overset/hybrid method.

Forward Flight

Before assembling the final overset/hybrid code, each methodology is applied separately to an advancing UH-60A rotor blade ($M_T = 0.64$, $\mu = 0.36$). First, an unsteady hybrid calculation is presented where the far-field wake effects are supplied by the comprehensive code CAMRAD/JA [15]. Next, the description of the wake is generalized by modeling the wake using the vorticity embedding method.

Isolated Blade Hybrid Solution: For this study, the wake inflow effects and the torsional deformation of the blade are obtained from the comprehensive code. This solution gives "partial angle of attack" information, which includes the far wake and aeroelastic effects at user specified radial and azimuthal locations. These angles are input into the hybrid solution as angle of attack corrections at every time step of the solution process. The blade surface rotates in pitch according to the "partial angle of attack" information as the rotor blade rotates around the azimuth. The time step chosen for this hybrid calculation is 0.025 which corresponds to approximately 0.05 degree/time step.

Since the wake inflow effects are specified as an angle of attack correction, it is sufficient to grid only one blade. The single block grid is characterized by 213 points in the wrap-around direction (144 points on the airfoil surface), 56 points in the normal direction and 26 points in the radial direction (19 on the blade). The normal distance of the first grid point from the blade surface is $0.00002c(r)$. The inner viscous grid is comprised of 40 points in the normal direction which places the outer boundary at approximately one chord. Figure 4 shows a schematic of the radial section of the hybrid computational C-H grid with the viscous and the inviscid zones. It is noteworthy that the inner zone extends to the downstream boundary of the C-grid which obviates the need to model the near wake using vorticity embedding (the far wake is accounted for in the angle of attack correction).

Figures 5 and 6 compare the predicted sectional lift and moment coefficients along the azimuth with CAMRAD/JA solutions, respectively. The predicted results are compared with the comprehensive code solutions to show that the unsteady load distributions are consistent with the impressed partial inflow. The lift coefficient compares well with the results of the comprehensive code. However, the moment coefficient comparison is not satisfactory. These differences may be attributed to the prediction of the blade aerodynamics (i.e. table lookup vs. CFD). The accuracy of pitching moment prediction is a concern and will be addressed in a later section of this paper.

Potential Overset Solution: In the previous unsteady hybrid solutions, the wake inflow effects were obtained from CAMRAD/JA solutions. In order to eliminate the dependence of the CFD solver on external wake models, the vorticity embedding concept is used in conjunction with an overset grid methodology. The advantages of using an overset method have been discussed in Ref. 11. For forward flight, a 360° H-H grid is used to convect the Lagrangian wake markers and define the vortical velocity field. A body-fitted C-H grid is used near the blade for a better representation of the flow near the surface. In this study, only one blade is resolved and the other blades are represented using lifting lines [9]. This is a simplification and not a limitation of the method, all four blades could be resolved using separate C-H grids.

For this calculation, the C-H grid consists of 103 points in the wrap-around direction (65 points on the surface), 20 points in the normal direction and 26 points in the radial direction (19 on the blade). The 360° H-H grid consists of 75 points in the azimuthal direction, 44 points in the normal direction and 26 points in the radial direction. The radial locations of the inner and outer grids are aligned. However, the solver is capable of handling staggered grids as well.

Figure 7 shows a radial cross-section of the overset grids. Only a portion of the 360° H-H grid is shown in the figure. The Lagrangian wake markers are convected in the H-H grid. Each wake sheet consists of 90 nodes in the azimuthal direction and 19 nodes along the radial direction which correspond to the radial grid locations. The markers originate from the trailing edge of the resolved blade and from the location of the lifting lines. New markers are introduced at the rotor plane at 4 degree intervals. However, the total number of markers are maintained constant during the computation. The circulation values of the marker nodes are updated every degree of azimuth. At present, the marker nodes convect with the freestream velocity (rotational + forward). In these calculations, the self-induced velocity is not taken into account. The vortical velocity is updated every time step (i.e. 0.2 degrees).

Calculations were performed for an advancing UH-60A helicopter rotor. Initially, the blade starts pitching and flapping according to the trim conditions and the wake develops in time as the blade rotates in az-

imuth. At every time step, the inner C-H grid rotates in pitch according to the pitch distribution and the hole boundaries are updated. The transfer of potential between the C-H and the H-H grids are performed at every time step in an explicit manner. Figure 8 shows the time evolution of the section normal force coefficient at $r/R = 0.675$. Periodic convergence occurs after three rotor revolutions.

The continuity of the interpolated quantities (in this case the velocity potential) across the overset boundaries can be visualized. Figure 9 shows the velocity potential contours on the overset grid at $r/R = 0.675$. As seen in the figure, the potential information is transferred smoothly across the grid interfaces and the contours are nearly coincident in the inner and outer regions of the intersecting grids.

Figures 10 and 11 compare the predicted sectional lift and moment coefficients along the azimuth with CAMRAD/JA solutions, respectively. The lift is higher in the current computations at all the radial stations on the retreating side. This clearly shows that the wake models of the comprehensive code and the present overset method are quite different and the comprehensive code predicts larger inflow due to the wake than the present wake system, particularly on the retreating side. Significant differences are noticed in the pitching moment variation at all radial stations. As with the hybrid results, some of the differences may be attributed to the blade aerodynamics.

To further evaluate the overset method, the advance ratio was reduced to 0.3 which matches the flow conditions for the experimental results of Lorber [16]. The torsional deformation information and the blade motion definition are obtained from the experimental data. For several radial locations, Fig. 12 compares the computed sectional normal force coefficients along the azimuth with experimental data. These solutions compare favorably well at the outboard radial stations. However, significant differences are observed at $r/R = 0.675$, particularly on the retreating side. In the experiment, Lorber reported a strong occurence of dynamic stall on the inboard portions of the blade. Since our potential model is not capable of predicting separation effects, significant differences at these locations would be expected.

Airfoil Study

This final section addresses the ability to accurately predict pitching moment. Simple harmonic airfoil oscillations (pitch and plunge) have been chosen as test cases to study the unsteady characteristics of these CFD methods. Although both the hybrid and overset methods have been evaluated, only overset results will be presented here. Computed results are compared with Theodersen's thin airfoil theory as well as single block C-grid solutions.

For these computations, a NACA 0006 airfoil is used to minimize thickness effects. The freestream Mach number is 0.1. The two-grid overset system consists of a body fitted C-grid enclosed by an outer H-grid. The C-grid has 103 points in the wrap-around direction (65 points on the airfoil surface) and 20 points in the normal direction. The H-grid consists of 146 points in the streamwise direction and 59 points in the normal direction. For these two-dimensional calculations, three radial planes are used where the spanwise flux derivatives are equated to zero.

To determine the accuracy limit of the time increment, a series of runs are performed at a reduced frequency (based on semi-chord) of 0.1 for different time step sizes. The accuracy limit is found to be a time step corresponding to approximately 6000 steps/cycle of oscillation. This accuracy time step limit decreases at higher reduced frequencies. That is, the lift and moment predictions are less sensitive to the time step at higher frequencies. Next, a series of runs are performed for a range of reduced frequencies (0.1 - 1.0) using a fixed time step corresponding to 6280 steps/cycle.

For simple harmonic pitching (2° amplitude), Fig. 13 compares the predicted unsteady lift and pitching moment solutions with the single block result and theory. The overall comparison between the computational solutions and the theory is good. However, the errors in the lift and pitching moment are higher in the case of overset solutions compared with the single block results. This clearly shows that there are additional errors introduced by oversetting grid topologies.

For simple harmonic plunging($0.1c_r$ amplitude), Fig. 14 compares the predicted unsteady lift and moment solutions with the single block result and theory. The errors in the phase of the pitching moment are higher in the overset solutions compared with the single block results. As with the pure pitching case, it appears that degradation of solution accuracy occurs when overset grid topologies are employed. Furthermore, this study shows that at low reduced frequency (corresponding to the rotor blade frequency) the most sensitive unsteady parameter is the phase of the pitching moment.

Concluding Remarks

An overset/hybrid method is being developed in an effort aimed at overcoming the physical and practical limitations of single-model flow solvers. Utilizing the experience of developing the hover overset/hybrid code, this paper addresses unsteady and forward flight appli-

cations.

Previous hover work has demonstrated the ability to predict drag and stall onset with these techniques. In this paper, hybrid computations of an advancing rotor blade have been performed. These computations demonstrated the ability to interface an inner hybrid solver to the vortex lattice model contained in a comprehensive code and obtain lift variations and distributions that are consistent with the impressed partial inflow. Overset computations have also been performed for a high advance-ratio rotor. These computations demonstrated the ability to predict the entire rotor/wake flow system independent of an external wake model. Good convergence and comparisons with available lift data were obtained. These results also identify moment prediction inaccuracies, the full nature of which are not currently understood. Computations of classical, unsteady, pitching and plunging airfoil solutions have been performed and these show large moment phase errors associated with the present oversetting implementation.

The present work demonstrates the unsteady overset rotor/wake and local blade hybrid capabilities required to develop the unsteady overset/hybrid method. This approach should yield a method with the speed, versatility and accuracy required of an engineering tool. Experience has shown that achieving reliable accuracy is the most difficult part of such a development. The present work is not the first to show that it is especially difficult to achieve pitching moment accuracy. It does underline the importance of classical unsteady airfoil analyses in the development and testing of new methods.

Acknowledgments

This research was supported by contract DAAJ02-96-C0033 (DoD SBIR). We would like to thank Dr. Joon Lim for his assistance in obtaining CAMRAD/JA solutions. Computations were performed at the Numerical Aerospace Simulation Facility at NASA Ames Research Center and at the DoD High Performance Computing Center in Waterways Experiment Station, MS.

References

[1] Strawn, R. C., and Caradonna, F. X., "Conservative Full Potential Model for Unsteady Transonic Rotor Flows," *AIAA Journal*, Vol. 25, No. 2, p193, February 1987.

[2] Strawn, R. C., and Tung, C., "Prediction of Unsteady Transonic Rotor Loads With a Full-Potential Rotor Code," 43rd Annual Forum of the American Helicopter Society, St. Louis, MO, May 18-20, 1987.

[3] Bridgeman, J. O., Prichard, D. and Caradonna, F. X., " The Development of a CFD Potential Method for the Analysis of Tilt-Rotors," American Helicopter Society Technical Specialists Meeting on Rotorcraft Acoustics and Fluid Dynamics, Philadelphia, PA, Oct. 15-17, 1991.

[4] Wake, B. E. and Sankar, L. N., " Solutions of the Navier-Stokes Equations for the Flow about a Rotor Blade, " *Journal of the American Helicopter Society*, Vol. 34, No. 2, April 1989, pp. 13-23.

[5] Berezin, R. C., " A Coupled Navier-Stokes/Full-Potential Analysis for Rotors," PhD Thesis, Georgia Institute of Technology, Atlanta, GA, 1995.

[6] Bangalore, A., " Computational Fluid Dynamic Studies of High Lift Rotor Systems Using Distributed Computing," PhD Thesis, Georgia Institute of Technology, Atlanta, GA, 1995.

[7] Ahmad, J. and Duque, E. P. N., " Helicopter Rotor Blade Computation in Unsteady Flows Using Moving Embedded Grids, " 12th AIAA Applied Aerodynamics Conference, Colorado Springs, CO, June 1994.

[8] Ramachandran, K., " Free Wake Analysis of Helicopter Rotor Flows in Hover using a Finite Volume Technique," PhD Thesis, University of Tennessee, Knoxville, 1987.

[9] Ramachandran, K. and Caradonna, F. X., " The Use of CFD for the Free-Wake Computation of Flows over General Multi-Bladed Rotors," American Helicopter Society Specialist Meeting on Aeromechanics Technology and Product Design, Bridgeport, CT Oct. 11-13, 1995.

[10] Moulton, M. A., Ramachandran, K., Hafez, M. M. and Caradonna, F. X. "The Development of a Hybrid CFD Method for the Prediction of Hover Performance." American Helicopter Society Specialist Meeting on Aeromechanics Technology and Product Design for the 21st Century, Bridgeport, CT, Oct. 11-13, 1995.

[11] Moulton, M. A., Bridgeman, J. O. and Caradonna, F. X., " Development of an Overset/Hybrid CFD Method for the Prediction of Hovering Performance," American Helicopter Society 53rd Annual Forum, Virginia Beach, VA, Apr. 29-May 1, 1997.

[12] Srinivasan, G. R., Baeder, J. D., Obayashi, S. and McCroskey, W. J., " Flowfield of a Lifting Rotor in Hover: A Navier-Stokes Simulation," *AIAA Journal*, 30, No. 10, October 1992, pp. 2371-2378.

[13] Steger, J. L., Dougherty, F. C. and Benek, J. A., "A Chimera Grid Scheme.", *Advances in Grid Generation*, K. N. Ghia and U. Ghia, eds., sponsored by the Fluids Engineering Division of ASME, 5, (June 1985):59-69.

[14] Lorber, P. F., Stauter, R. C., Pollack, M. J. and Landgrebe, A. J., "A Comprehensive Hover Test of the Airloads and Airflow of an Extensively Instrumented Model Helicopter Rotor." US Army Aviation Systems Command (USAAVSCOM) TR 91-D-16E, October 1991.

[15] Johnson, W., "A Comprehensive Analytical Model of Rotorcraft Aerodynamics and Dynamics, Johnson Aeronautics Version Volume I and II," Johnson Aeronautics, 1988.

[16] Lorber, P. F., " Aerodynamic Results of a Pressure-Instrumented Model Rotor at the DNW, " American Helicopter Society 46th Annual Forum, Washington, D. C., May 21-23, 1990.

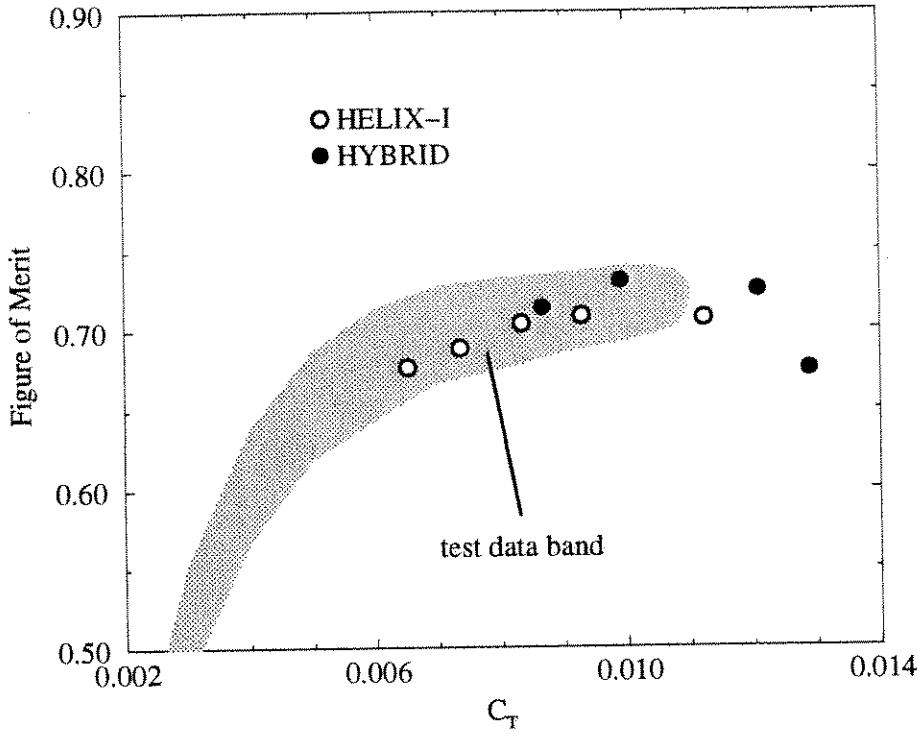

Figure 1: Comparison of hybrid performance prediction with experimental data and HELIX-I solutions (Apache rotor, $M_T = 0.63$, $Re_c = 2.75 \times 10^6$)

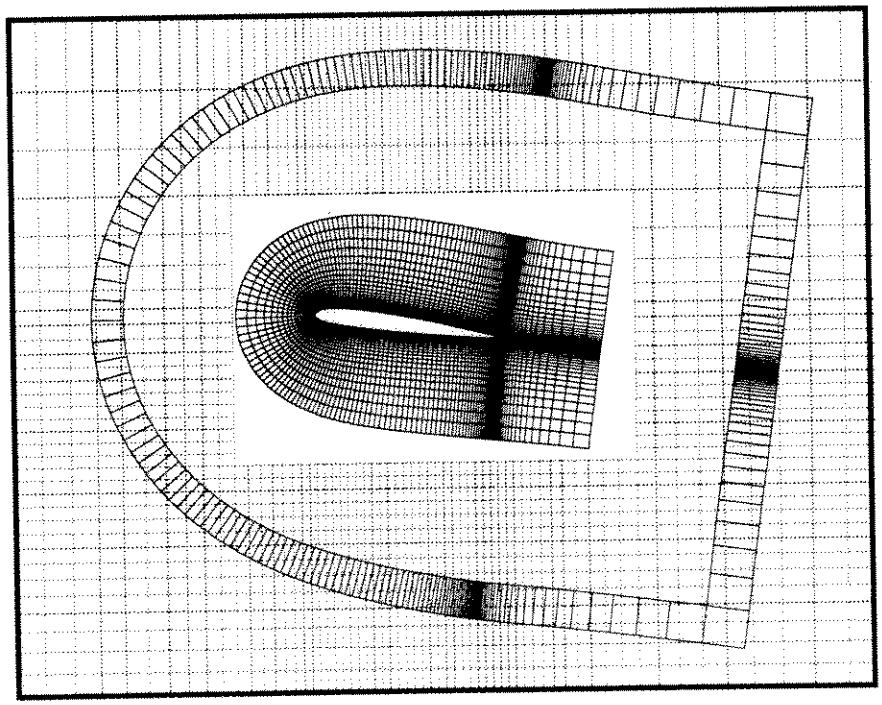

Figure 2: Overset/hybrid grids near the blade surface showing the hole boundary of H-grid (UH-60A rotor, $\theta_c = 10.0°$)

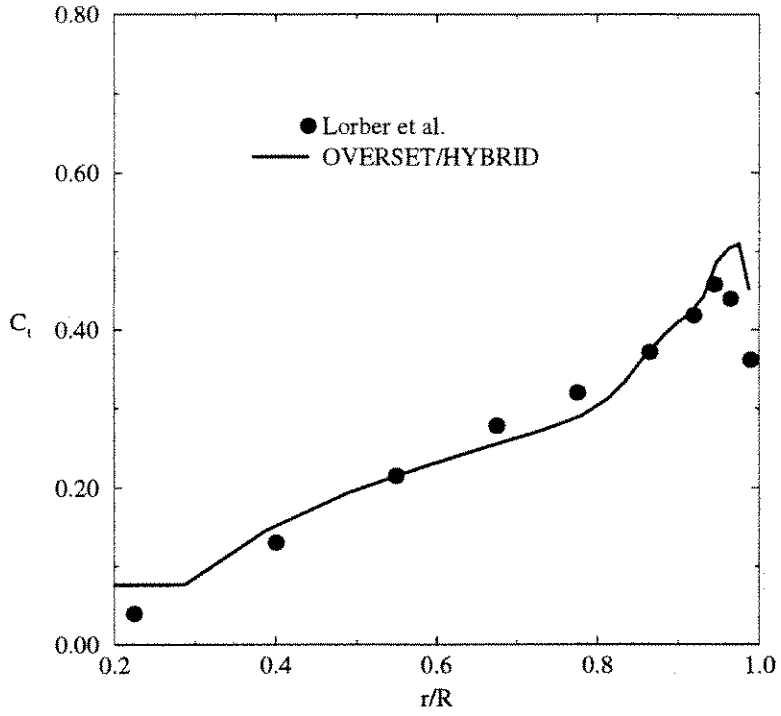

Figure 3: Comparison of computed loading from overset/hybrid method with experiment (hovering UH-60A rotor, $\theta_c = 10.0°$, $M_T = 0.63$)

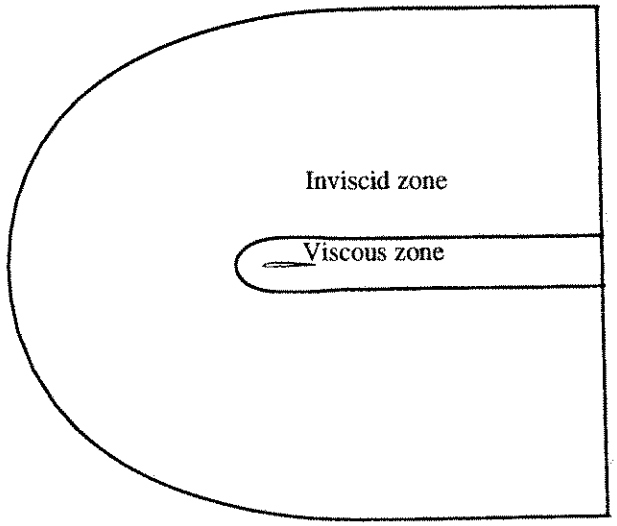

Figure 4: A schematic showing the viscous and inviscid zones for a hybrid grid

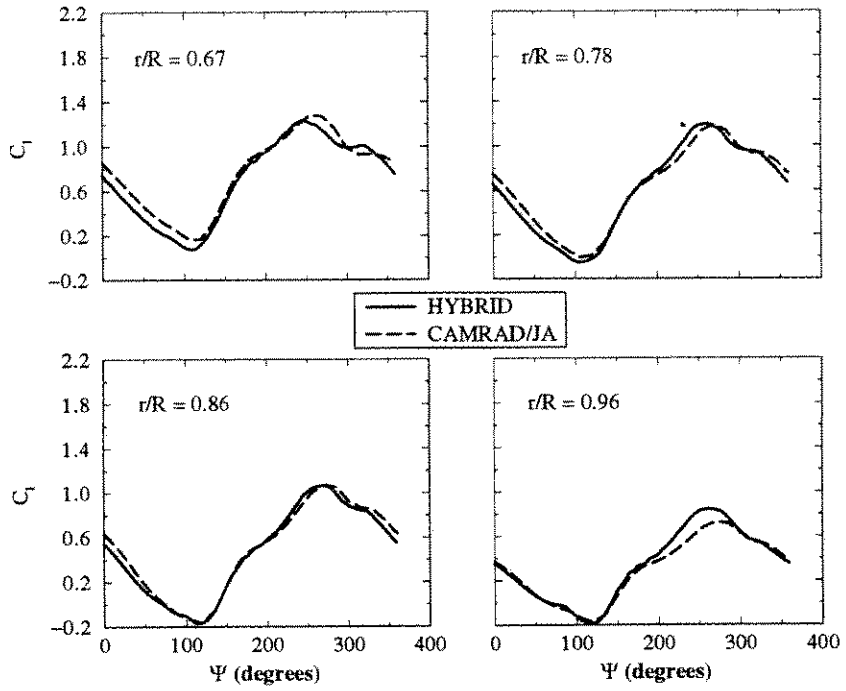

Figure 5: Comparison of predicted sectional lift coefficient along the azimuth with CAMRAD/JA solutions (UH-60A rotor, $M_T = 0.64, \mu = 0.36$)

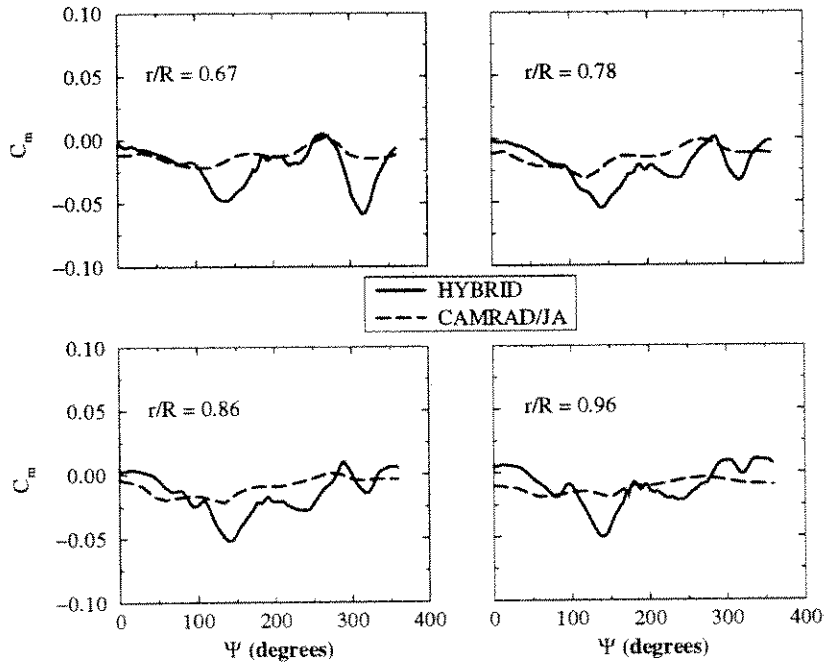

Figure 6: Comparison of predicted sectional moment coefficient along the azimuth with CAMRAD/JA solutions (UH-60A rotor, $M_T = 0.64, \mu = 0.36$)

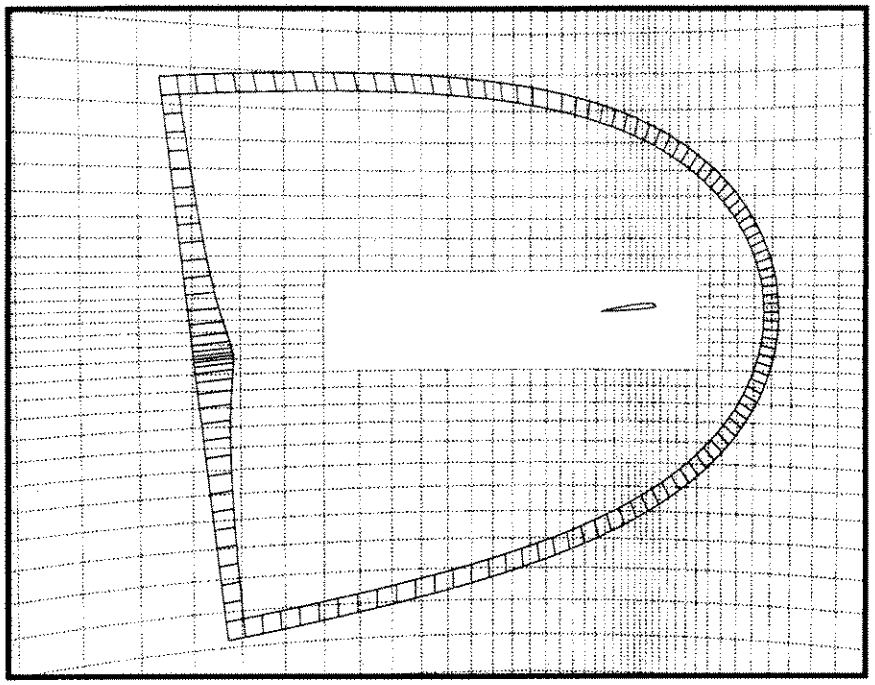

Figure 7: Overset grids near the blade surface at $r/R = 0.675$

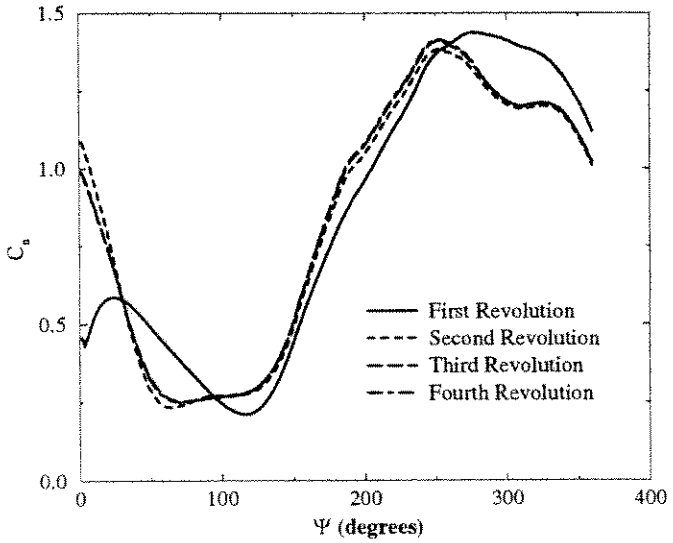

Figure 8: Time evolution of the normal force coefficient at $r/R = 0.675$ for the unsteady overset method (UH-60A rotor, $M_T = 0.64$, $\mu = 0.36$)

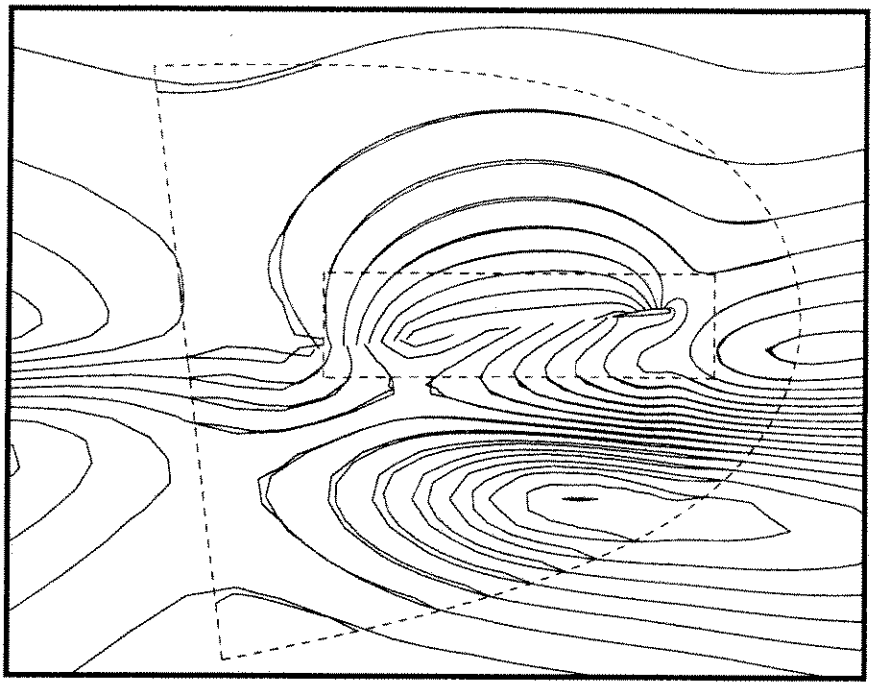

Figure 9: Contours of velocity potential at $r/R = 0.78$ for the unsteady overset method (UH-60A rotor, $M_T = 0.64$, $\mu = 0.36$)

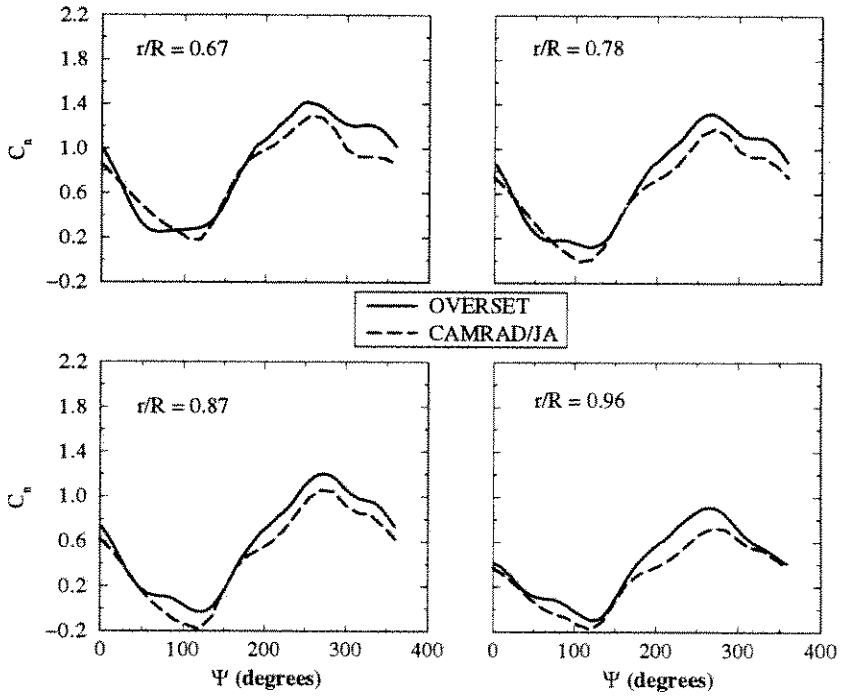

Figure 10: Comparison of predicted sectional normal force coefficient along the azimuth with CAMRAD/JA solutions (UH-60A rotor, $M_T = 0.64, \mu = 0.36$)